Energy Reports 7 (2021) 7445–7459

Contents lists available at ScienceDirect

Energy Reports

journal homepage: www.elsevier.com/locate/egyr

Research paper

Simultaneous analysis of frequency and voltage control of the interconnected hybrid power system in presence of FACTS devices and demand response scheme

Sudhanshu Ranjan [a], Abdul Latif [a], Dulal Chandra Das [a], Nidul Sinha [a], S.M. Suhail Hussain [b], Taha Selim Ustun [c], Atif Iqbal [d,*]

[a] Department of Electrical Engineering, National Institute of Technology Silchar, Assam, India
[b] Department of Computer Science, National University of Singapore (NUS), 119077, Singapore
[c] Fukushima Renewable Energy Institute, AIST (FREA), Koriyama, Japan
[d] Department of Electrical Engineering, Qatar University, Doha, Qatar

ARTICLE INFO

Article history:
Received 26 August 2021
Received in revised form 21 October 2021
Accepted 25 October 2021
Available online 14 November 2021

Keywords:
Parabolic trough solar power system (PSP)
Dish-stirling solar power system (DSP)
Dynamic voltage restorer (DVR)
Demand response scheme (DRS)
Mine blast algorithm (MBA)

ABSTRACT

This work confers the simultaneous analysis of voltage and frequency control of the 3-area interconnected hybrid power system (IHPS) consisting of parabolic-trough solar power system (PSP), wind power system (WPS) and dish-stirling solar power system (DSP) under the paradigm of microgrid. The speculated result of the IHPS is presented and analyzed considering real and reactive power as the function of both voltage and frequency. 9The proposed IHPS under investigation has been mathematically modeled for direct coupling like active power–frequency and reactive power–voltage relationships and cross coupling like active power–voltage and reactive power–frequency relationships. The system responses under different operating conditions have been investigated to see the cross-coupling behavior of the proposed IHPS in the presence of voltage compensating devices like dynamic voltage restorer (DVR) and Static Synchronous Compensator (STATCOM). Further, Demand Response Scheme (DRS) as a frequency control strategy has been considered to enhance the system stability. System responses have been critically analyzed under Mine Blast Algorithm (MBA) based proportional–integral–derivative (PID) controllers

1. Introduction

The concentrated solar power system (CSP) will play a vital role in the coming days to address the global warming and the future energy crisis (Ellingwood et al., 2019; Wang et al., 2019). Currently, there are four common CSP technologies, out of which parabolic-trough solar power system (PSP) is the most developed and commercially proven (Taqiyeddine et al., 2013) while dish-Stirling solar power system (DSP) reported to provide electricity with an efficiency of 32.17% (Praene et al., 2016). These technologies are being hybridized to enhance the energy harnessed and hence to enhance further CSP deployment (Ellingwood et al., 2020). Additionally, hybridization may reduce the capital cost and CO_2 emission, improve the reliability and efficiency, and enhance dispatch ability & flexibility (Powell Kody et al., 2017).

Notwithstanding the advantages of CSP, variable output power of DSP and PSP in a hybrid power system (HPS) may cause system voltage and frequency fluctuations which must be smoothened to ensure stability of HPS (Ju et al., 2017). The renewable energy units, WPS, DSP and PSP are equipped with squirrel cage induction generator (SCIG), whereas synchronous generator is coupled with diesel generator. SCIG has simple construction, rugged nature and low maintenance cost, and hence has been a prevalent choice for WPS, DSP and PSP operation (Hussain et al., 2017; Sharma et al., 2013b). Nonetheless, SCIG needs reactive power for developing magnetic field, it reduces the power factor and has lower efficiency (Fukami et al., 2004). This may create voltage stability problem when SCIG is connected in HPS.

In this context, reactive power compensating device, particularly static var compensator (SVC) has been used for catering the reactive power demand in SCIG coupled wind turbine diesel based HPS (Bansal and Bhatti, 2008; Wessels et al., 2013; Sitthidet et al., 2010). Further, controllers' parameters employed with SVC and automatic voltage regulator (AVR) are tuned by genetic algorithm (Wessels et al., 2013). The system performance has been examined considering random load perturbation on the system, but the reactive power required by the SCIG is kept fixed. Nonetheless, fixed reactive power supply may not meet the reactive power demand of the SCIG as the output power from

* Corresponding author.
E-mail address: atif.iqbal@qu.edu.qa (A. Iqbal).

https://doi.org/10.1016/j.egyr.2021.10.100

the WPS varies to some extent due to wind variation. Therefore, appropriate reactive power compensating devices for such hybrid system can be explored. To this end, Static Synchronous Compensator (STATCOM) has been employed in Sharma et al. (2013a) for the wind–diesel based HPS. Three different generators like SCIG, permanent magnet synchronous generator (PMSG) and permanent magnet induction generator (PMIG) are employed in HPS model and performance of these generators are compared. Nevertheless, coordinated control could be developed by optimizing the STATCOM and AVR control parameters simultaneously considering the realistic features of reactive power generation and demand. Moving forward, it is learnt that dynamic voltage restorer (DVR) (Priyavarthini et al., 2018; Wang et al., 2006; Meena et al., 2017) like SVC and STATCOM attenuates the fluctuation in voltage profile significantly and have the capability to provide the required amount of voltage for proper system functioning. Recently, DVR has been used (Meena et al., 2017) for improving the unbalanced 3-phase voltage profile. Result is satisfactory. However, optimizing the controllers' (current and voltage) parameters would improve the system performance further.

In an IHPS, in addition to voltage deviation, frequency fluctuation is also common phenomenon because the power output from the renewable energy units like WPS, DSP, PSP are dependent weather condition beside load variation in system. And hence frequency control is also an important topic. Several works devoted in this direction (Lee and Wang, 2008; Senjyu et al., 2005; Latif et al., 2021, 2020b; Shankar and Mukherjee, 2016). Different auxiliary units like battery and aqua-electrolyzer (Lee and Wang, 2008; Senjyu et al., 2005) have been employed for leveling the frequency fluctuations in HPS. Proportional–integral (PI) controller has been considered in Senjyu et al. (2005) to eradicate the mismatch in the active power generation and demand of the system. However, controllers' parameters need to be optimized as fixed parameters may provide satisfactory performance. Different controllers PI, proportional–integral–derivative (PID), fractional order proportional–integral–derivative (FOPID), etc. has been reported in Latif et al. (2021, 2020b) in respect to frequency control of hybrid power system. However, due to simplicity during implementation PID controllers are suitable for IHPS application. Recently, demand response schemes (DRS) have been recognized and employed in HPS for frequency control (Bao et al., 2015; Huang and Li, 2013; Barik and Das, 2019; Pourmousavi and Nehrir, 2014; Li et al., 2021; Pourmousavi and Nehrir, 2012; Latif et al., 2020a; Zhu et al., 2017). Devices used in DRS are normally non-critical loads (NCL) like air conditioners, freezes, different types of electric water heaters (EWH) and so on.

The change in frequency and voltage due to change in active power and reactive power respectively can be interpreted as the direct coupling as active power–frequency and reactive power–voltage. However, this phenomenon is useful in very large power system. On the other hand, cross-coupling can be significantly observed in the small hybrid power system which cannot be overlooked (Avisha and Das, 2016). However, this cross-coupling of Q–f and P–V is not as large as the direct-coupling of Q–V and P–f but this phenomenon is important and essential to be observed in small hybrid power system.

Though there are several literatures available on the direct coupling effect, only few papers have investigated the cross-coupling effect or both. Authors in Avisha and Das (2016) have investigated in details both the direct and cross coupling effect in single wind–diesel hybrid power system as well as interconnected two area system. The eigenvalue analysis has been performed using classical control method and peak deviation of V and f has been examined which implies that the changes in Q and P affect the system f and V, respectively, along with the direct coupling effect. However, application of meta-heuristic based-on control strategy needs to be explored. The combined effect of load frequency control (LFC) and AVR model in 2-area HPS comprising of flywheel and wind turbine unit in area 1 and 2 respectively, while thermal generation, micro-turbine turbine unit in both the area has been studied in Othman and El-Fergany (2018). The performance of model predictive control strategy has been compared with that of classical and genetic algorithm (GA) based control techniques. Nevertheless, performance of the hybrid model could have been appraised considering of realistic features.

Therefore, a clear speculation of any small hybrid power system is that the cross-coupling phenomenon can be investigated along with its direct coupling analysis. Thus, the above literature survey motivates to develop the hybrid power system and to analyze the system responses under direct and cross coupling relation. This has been the impetus towards development of IHPS model and investigate the simultaneous control of voltage and frequency of the system in presence of three different renewable energy units like WPS, DSP and PSP. Beside three main sources, diesel engine generators and some energy storing devices are considered like superconducting magnetic energy storage system (SMES), ultra-capacitor (UC), and battery energy storage system (BESS). Investigation like, direct and the cross-coupling phenomena in the presence of DRS and voltage compensating flexible AC transmission system (FACTS) devices such as STATCOM and DVR in such an IHPS is a novel work. This FACTS units are integrated with the PID controllers to control the voltage profile as per the requirement whose parameters are optimally adjusted through the algorithmic techniques i.e., MBA. Moreover, DRS are also considered to reduce the fluctuation in the frequency of the system. The prime contributions in this work are as follows:

(i) Simultaneous control of frequency and voltage of 3-area IHPS with renewable generating units like WTG, PSP and DSP in each respective are along with other auxiliary units has been studied for the first time.

(ii) Use of STATCOM and DVR for reactive power compensation and compare the performance in terms of dynamic responses for voltage stability.

(iii) Analysis of cross-coupling between frequency and voltage for such IHPS has been done for the first time.

(iv) Application of DRS strategy and its analysis for maintain frequency stability of the system.

(v) Use of MBA for optimum tuning of control parameters for maintaining the stable concurrent voltage–frequency equilibrium under various operating points.

2. Mathematical modeling of IHPS

In this work, a HPS includes the renewable energy sources (RESs) like WPS, DSP, and PSP which has been illustrated in Fig. 3. The proposed HPS has been mathematically developed keeping the direct and cross coupling effect of the system parameters into the consideration. The main objective to develop such a HPS is to see the cross impact of reactive power deviation over frequency and active power deviation over voltage in addition to the direct impact of active power deviation on frequency and reactive power deviation on voltage. The efficacy of the proposed system is investigated through the system voltage and frequency deviation limit. The considered system is operated and controlled within the permissible limit of the voltage ($V_{rated} = 440$ V) and the frequency ($f = 50$ Hz). The system has included the diesel generator comprising of SG to provide the required power under non-accessibility of the main sources. Initially, the isolated HPS (as one area) has been developed considering the linear transfer function model of each device and then finally 3 area interconnected HPS has been developed which are shown in Figs. 3(a), 3(b) and 3(c) respectively.

The proposed 3A-IHPS has been investigated under two voltage compensating devices like STATCOM and DVR to see their effectiveness in controlling the voltage deviation. Meanwhile, their comparative study clarifies the better device to compensate the reactive power of the IHPS. In addition to it, the proposed system has also been investigated under DRS to control the frequency irrespective of degree of penetration of the RESs in the system.

Under balance or normal operating condition, the deviation in frequency and voltage is zero. The active power and the reactive power of the system could be illustrated by the following Eqs. (1) and (2) respectively under steady state condition. Here energy storage system (ESS) delivers power during deficit of power in the system and it draws power during surplus power in the system. Insertion and removal of the NCLs as DRS are practiced in the discrete order to maintain the stable equilibrium operating point of the system. The available aggregate NCLs is very large for smooth control of the frequency deviation.

$$P_{IG} + P_{SG} \pm P_{ESS} = P_{NCL} + P_L \tag{1}$$

$$Q_{SG} + Q_{VCD} = Q_L + Q_{IG} \tag{2}$$

Under unbalance or transient condition, the deviation in frequency occurs as overall generated active power is not equal to that of load demand of the system and deviation in voltage occurs as the load reactive power does not match with the generated reactive power of the system. Therefore, the voltage deviation and frequency deviation can be expressed by the Eqs. (3) and (4) (Sitthidet et al., 2010) respectively.

$$\Delta V(s) = \frac{K_v}{1+sT_v}\left[\Delta Q_{SG}(s) + \Delta Q_{VCD}(s) - \Delta Q_{IG}(s) - \Delta Q_L(s)\right] \tag{3}$$

$$\Delta f = \frac{K_f}{1+sT_f}\left[\Delta P_{IG} + \Delta P_{SG} \pm \Delta P_{ESS} \pm \Delta P_{NCL} - \Delta P_L\right] \tag{4}$$

Reactive power of the SG can be written as Eq. (5) (Sharma et al., 2013a)

$$Q_{SG} = \left(E_q V\cos\delta - V^2\right)/x_d \tag{5}$$

Under small perturbation, the change in reactive power of the SG can be calculated by differentiating the Eq. (5), and which can be expressed by (6).

$$\Delta Q_{SG}(s) = \frac{1}{x_{d'}}\left[V\cos\delta\,\Delta E_q' + E_q'\cos\delta\,\Delta V - 2V\Delta V + VE_q'\sin\delta\right] \tag{6}$$

Further Eq. (6) can be written as Eq. (7):

$$\Delta Q_{SG} = \frac{V\cos\delta}{x_{d'}}\Delta E_q' + \frac{E_q'\cos\delta - 2V}{x_{d'}}\Delta V + \frac{VE_q'\sin\delta}{x_{d'}}\Delta\delta \tag{7}$$

And then it can be written in Laplace form through Eq. (8):

$$\Delta Q_{SG}(s) = K_1\Delta E_q'(s) + K_2\Delta V(s) + K_3\Delta\delta(s) \tag{8}$$

where, $K_1 = \frac{V\cos\delta}{x_{d'}}$, $K_2 = \frac{E_q'\cos\delta - 2V}{x_{d'}}$, and $K_3 = \frac{VE_q'\sin\delta}{x_{d'}}$

At small perturbation, voltage of the armature of synchronous generator deviates from its base value. That is why the equation of linkage flux (Avisha and Das, 2016) under small perturbation can be mathematically expressed by the Eq. (9).

$$\frac{d}{dt}\Delta E_q = \frac{\Delta E_{fd} - \Delta E_q}{sT_{d0}'} \tag{9}$$

where, $\Delta E_q = \frac{x_d}{x_d{}'}\Delta E_q' - \frac{x_d - x_d{}'}{x_d{}'}\cos\delta\,\Delta V + \frac{x_d - x_d{}'}{x_d{}'}V\sin\delta\,\Delta\delta$

By solving Eq. (9), it can be expressed as:

$$\Delta E_q(s) = \frac{1}{1+sT_G}\left\{K_4\Delta E_{fd}(s) + K_5\Delta V(s) + K_6\Delta\delta(s)\right\} \tag{10}$$

where, $K_4 = \frac{x_d}{x_d{}'}$, $K_5 = -\frac{x_d - x_d{}'}{x_d{}'}\cos\delta$, and $K_6 = \frac{x_d - x_d{}'}{x_d{}'}V\sin\delta$

In similar manner, the deviation in the active power of the SG (Avisha and Das, 2016) can be written as:

$$\Delta P_{SG}(s) = K_7\Delta E_q'(s) + K_8\Delta V(s) + K_9\Delta\delta(s) \tag{11}$$

where, $K_7 = \frac{V\sin\delta}{x_{d'}}$, $K_8 = \frac{E_q'\sin\delta}{x_{d'}}$, and $K_9 = \frac{VE_q'\cos\delta}{x_{d'}}$

Similarly, real and reactive power of the induction generator (Avisha and Das, 2016) can be expressed by the following Eqs. (12), and (13) respectively.

$$\Delta P_{IG}(s) = K_{10}\Delta V(s) + K_{11}\Delta P_{IP}(s) \tag{12}$$

$$\Delta Q_{IG}(s) = K_{12}\Delta V(s) + K_{13}\Delta P_{IP}(s) \tag{13}$$

where,

$$K_{10} = \frac{2VR_Y}{(R_Y^2 + X_{eq}^2)}\left[1 + \frac{V^2(R_d/R_Y)(R_Y^2 - X_{eq}^2)}{(R_Y^2 + X_{eq}^2)\{2R_Y(P-P_c) + V^2\}}\right]$$

$$K_{11} = \frac{-V^2(R_Y^2 - X_{eq}^2)}{(R_Y^2 + X_{eq}^2)\{2R_Y(P-P_c) + V^2\}},$$

$$K_{12} = \frac{2VX_{eq}}{(R_Y^2 + X_{eq}^2)}\left[1 + \frac{2V^2(R_dR_Y)}{(R_Y^2 + X_{eq}^2)\{2R_Y(P-P_c) + V^2\}}\right]$$

$$K_{13} = \frac{2V^2X_{eq}R_Y}{(R_Y^2 + X_{eq}^2)\{2R_Y(P-P_c) + V^2\}}$$

$$R_d = \frac{r_2{}'}{s}(1-s),\ R_Y = R_d + r_e \qquad P_{IP} = P_c + \frac{2V^2R_d}{(R_Y^2 + X_{eq}^2)}$$

Eqs. (8), (9), and (10) provide the relation of the change in reactive power of the SG with the change in voltage and the change in load angle. Eq. (13) governs the relation of the reactive power of induction generator with the change in system voltage and the change in active power. These above-mentioned equations signify that the change in frequency or the change in active power will also affect the reactive power or voltage of the system. Similarly, Eqs. (11) and (12) show the impact of change in voltage overactive power or frequency of the SG and IG respectively. All the above-mentioned equations explicitly clarify the cross-coupling effect in the proposed HPS.

2.1. Voltage control strategies

2.1.1. Static synchronous compensator (STATCOM)

The STATCOM unit is leveraged to contain the voltage deviation of the WPS, DSP, and PSP based interconnected hybrid power system by minimizing the divergence between the reactive power generation and demand. The structural layout of the STATCOM has been shown in Fig. 1 (Sharma et al., 2013b).

The reactive power introduced by the STATCOM unit can be express as (Sharma et al., 2013b).

$$Q_{STAT} = K\left[V_{DC}{}^2B - V_{DC}VB\cos(\alpha - \partial) + V_{DC}G\sin(\alpha - \partial)\right] \tag{14}$$

Where, V represents bus voltage. V_{DC} represents capacitor's voltage. The extractable angle of fundamental voltage and the phase angle is represented by α and ∂ respectively. It is assumed that, the converter's losses and coupling transformer are zero, conductance (G) could be deliberated to be zero, where jB represents the coupling transformer's admittance. With reference voltage (V),

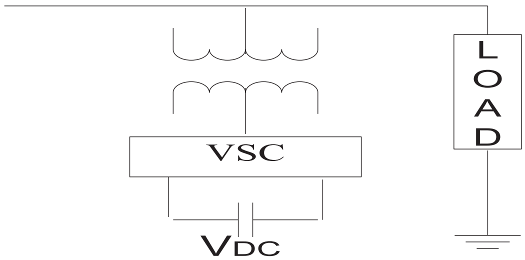

Fig. 1. Schematic diagram of STATCOM.

∂ becomes zero, hence, the Eq. (14) can be written as Eq. (15) (Sharma et al., 2013b).

$$\Delta Q_{STAT}(s) = K_{13}\Delta\alpha(s) + K_{14}\Delta V(s)$$
$$\text{where, } K_{13} = KV_{DC}VB\sin\alpha, K_{14} = -KV_{DC}VBCOS\alpha \tag{15}$$

2.1.2. Dynamic voltage restorer (DVR)

The utilization of power electronic based different FACTS units in the power network increases the capability to contain the various network parameters like voltage, frequency, and the flow of active and reactive power. DVR is a prominent FACTS unit which is connected in series could be leveraged to improve the power stability of the power network by enhancing stability margin. This unit could be widely applicable for various purposes like the alleviation of voltage sags, swells, decrease of voltage mismatch, harmonics filtering and the improvement of other power quality issues (Priyavarthini et al., 2018). In addition, this application has been utilized in South Carolina based 13 kV, 2 MVA power substation for the very first time. The fast-acting performance of DVR which consists of power electronics-based voltage source convertor (VSC), the series coupling transformer with one energy storage unit as depicted in Fig. 2. Considering the connection of DVR, the voltage injection of DVR is perpendicular to sensitive line current to stabilize the reactive power of the network. The dynamic control strategy of DVR lies by controlling both voltage magnitude and phase. The transfer function model of DVR could be formulated as Eq. (16) (Wang et al., 2006; Meena et al., 2017):

$$G_{DVR}(s) = \frac{2V_{CC}(R_{cd}L_ds + 1)}{L_dC_ds^2 + (R_{ld} + R_{cd})C_ds + 1} \tag{16}$$

2.2. Frequency control strategies

2.2.1. Demand response scheme (DRS)

DRS consisting of non-critical loads (NCLs) can smoothen the system frequency response through the proper management of upper and lower limit of the frequency deviation of all the available non-critical loads. The DRS has two segments for its operation: the devices used as NCLs in the scheme and the controlling part. Those devices are nonessential like electric heater, air conditioning machine, refrigerators and so on (Bao et al., 2015; Huang and Li, 2013; Barik and Das, 2019). Controlling scheme is required to keep the number of devices on and off as to control the consumed power by the devices according to the frequency control scheme. For smooth operation, number of the DRS can be incorporated to the system.

The important segment of DRS is the controlling scheme which operates on the basis of deviation in the system frequency (Pourmousavi and Nehrir, 2014; Li et al., 2021). A threshold deviation in frequency is considered to activate the noncritical loads of DRS. Here, the behavior of the NCLs will be in the discrete form as because all the devices will be either on or off. But the problem associated with the response in the discrete form can be overcome by designing and managing the threshold value of the frequency deviation of each device.

Total power (ΔP_{DRS}) of the DRS can be activated at particular time by estimating the power through the considered logic shown in Eqs. (18), and (19), where L_{DRS} and ΔP_{DRM} are assumed as the co-efficient and the total power of the DRS respectively.

The value of the co-efficient is optimized through the optimizing technique, and the maximum power is estimated on the basis of the contract of the DRS. The maximum deviation in the frequency for the operation of DRS is regulated through the utility. Here, in this system, the maximum deviation in frequency is considered as 0.05 Hz for the operation of DRS. In this work, the linear Laplace transfer function model of the water heater has been considered which is represented by the Eq. (17). Eq. (18) shows the total power of the DRS connected to the proposed system.

$$G_{WH}(s) = \frac{K_{WH}}{1 + sT_{WH}} \tag{17}$$

$$\Delta P_{DRS} = \begin{Bmatrix} \dfrac{\Delta f}{|\Delta f_m|}\Delta P_{DRM}, & -\Delta f_m \le \Delta f \le \Delta f_m \\ \dfrac{\Delta f}{|\Delta f|}\Delta P_{DRM}, & \text{otherwise} \end{Bmatrix} \tag{18}$$

$$\Delta P_{DRSi} = \begin{Bmatrix} \dfrac{\Delta f_i}{|\Delta f_m|}\Delta P_{DRMi} - L_{DRS}\Delta P_{tiei-i}, & -\Delta f_m \le \Delta f \le \Delta f_m \\ \dfrac{\Delta f_i}{|\Delta f_m|}\Delta P_{DRMi}, & \text{otherwise} \end{Bmatrix} \tag{19}$$

The abovementioned equations will establish the Laplace transformation-based transfer function of excitation system, distributed synchronous generator, induction generator and considered FACTS units (i.e., STATCOM, and DVR). Finally, by integrating all the above components together we develop an islanded hybrid power system as shown in Fig. 3(a), in which voltage and frequency fluctuation could be analyzed when the disturbances in the generation and the demanded load active and reactive power. First order transfer function model of one isolated HPS (area) is developed on the basis of above equations and shown in Fig. 3(b) whereas the complete block diagram of the interconnected hybrid power system comprising of three different isolated RESs is shown in Fig. 3(c). The required parameters of the proposed system are obtained from the available literature (Hussain et al., 2017; Sharma et al., 2013b; Bansal and Bhatti, 2008; Lee and Wang, 2008; Senjyu et al., 2005; Ranjan et al., 2018) and some values are calculated on the basis of above derived equations and summarized in Table 1.

3. Problem formulation

3.1. Formulation of the objective function

Different types of the objective functions can be considered to minimize voltage and frequency deviation and thus to control the system against any disturbance. Proper selection of the objective functions for the problems associated with simultaneous control of voltage and frequency plays an important role to get the feasible solution. In this study, integral time absolute error (ITAE) is considered for all four cases as this objective function substantiates its higher potential to control the system parameters as compared to all other objective functions like integral absolute error (IAE), integral square error (ISE) and integral time square error (ITSE). The simultaneous control of voltage and frequency becomes complex as frequency response of the system is slower

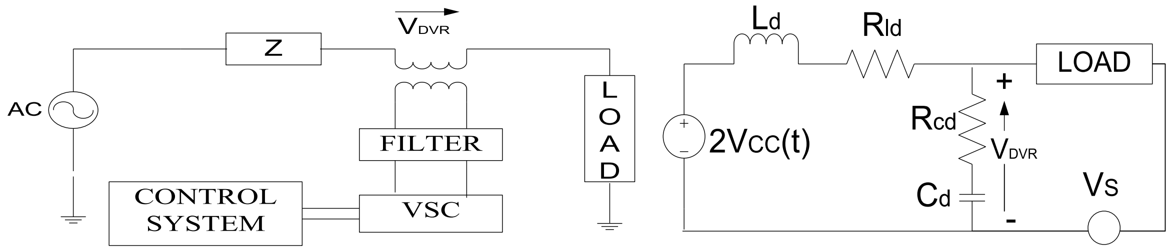

Fig. 2. Schematic with equivalent circuit structure of DVR.

Table 1
Numerical values of the system parameters (Hussain et al., 2017; Sharma et al., 2013b; Bansal and Bhatti, 2008; Lee and Wang, 2008; Senjyu et al., 2005; Ranjan et al., 2018).

System parameters	Symbols	values
Gain and time constant of wind turbine, parabolic trough, dish stirling respectively.	$T_W, T_{PSP}, T_{DSP} K_W, K_{PSP}, K_{DSP}$	1, 1.8, 1, 1.5 s., 1.8 s., 5 s.
Gain and time constant of battery energy storage system, ultracapacitor, and superconducting magnetic storage system.	$T_{BESS}, T_{UC}, T_{SMES}, T_{WH} K_{BESS}, K_{UC}, K_{SMES}, K_{WH}$	0.1, 0.2, 1, −0.003 s, 4 s, 3 s.
Gain and time constant of valve actuator and diesel engine.	$K_{VE}, K_{DE}, T_{VE}, T_{DE}$	1, 1, 0.05 s., 0.5 s.
Power transfer co-efficient.	a_{12}, a_{23}, a_{13}	−0.75, −0.33, −0.25.
Gain and time constant of synchronous generator, stabilizer, AVR, exciter, and voltage transfer of the system.	$T_G, T_F, T_A, T_E, T_V K_G, K_F, K_A, K_E, K_V$	1, 0.5, 40, 1, 0.6667, 0.75 s, 0.715 s, 0.05 s, 0.55 s, 0.00061 s.
Time constant parameters and delay angle of the STATCOM.	$K_1, K_2, K_3, K_4, K_5 T_\alpha, T_d, \alpha$	0.0002 s, 0.00167 s, 140.02^0.
Constant of the complete HPS for frequency and voltage analysis.	$K_{11}, K_{12}, K_{13}, K_{14}, K_{15} K_6, K_7, K_8, K_9, K_{10}$	6.23, −7.36, −2.30, 0.15, 0.79, −0.30, 2.40, 2.29, 5.97, 0.03, 0.84, 0.097, −0.444.

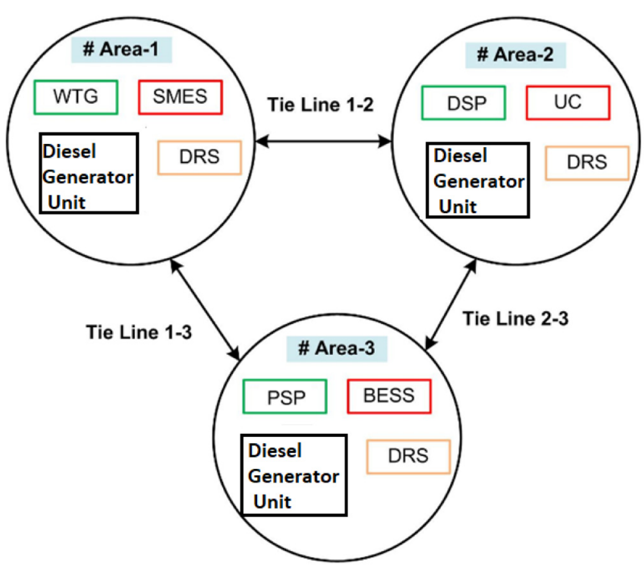

Fig. 3(a). Schematic diagram of the isolated HPS.

than that of the voltage response. In this study, scaling factor is used to develop the objective function depending on the disturbances in the reactive and active power of the system since the deviation in frequency and voltage is of different range. When the system is subjected to the reactive power change, n is multiplied with frequency deviation whereas scaling factor m is multiplied with voltage deviation when change in active power occurs. The range of m and n are taken in between 0 and 10.

$$J_1 = \int_0^T t\,(|\Delta f_i| + m\,|\Delta V_i|)\,dt \tag{20}$$

$$J_2 = \int_0^T t\,(|\Delta f_i| + n\,|\Delta V_i|)\,dt \tag{21}$$

where J_1 *and* J_2 given in Eqs. (20) and (21) are the objective functions modeled for active power change and reactive power change respectively. The optimized values of m and n for this study for different cases are different which have been discussed in result and discussions.

Here, the proposed system would be subjected to variation in the load as well as generation to examine the feasibility of the system which may lead to the deviation in voltage and frequency. That is why J_1 *and* J_2 are modeled and interfaced with PID controllers to minimize the deviations and to keep the system in stable equilibrium operating conditions. J_1 *and* J_2 are minimized keeping some constraints:

$$K_p^{\min} \le K_p \le K_p^{\max}$$
$$K_i^{\min} \le K_i \le K_i^{\max}$$
$$K_d^{\min} \le K_d \le K_d^{\max}$$

Proportional, Integral, and Differential controllers' gains for different sources connected in the system are ranging from 0–20. Fig. 3(d) represents the approach regarding implementation of MBA for optimizing the control parameters of PID Controllers. As such, there are eighteen control parameters (total 6 PID controllers) which are tuned by using MBA. ITAE of frequency deviations and voltage deviations in all three areas has been considered as the objective function. Then the MBA is employed to find the minimum possible value of the objective function and thereby optimum values of the controllers' gains.

3.2. Mine blast algorithm (MBA)

Mine blast algorithm initiates with the point known as the first shot point which can be expressed as x_0^f where f represents the no. of initial shot points varying from 1 to any defined number.

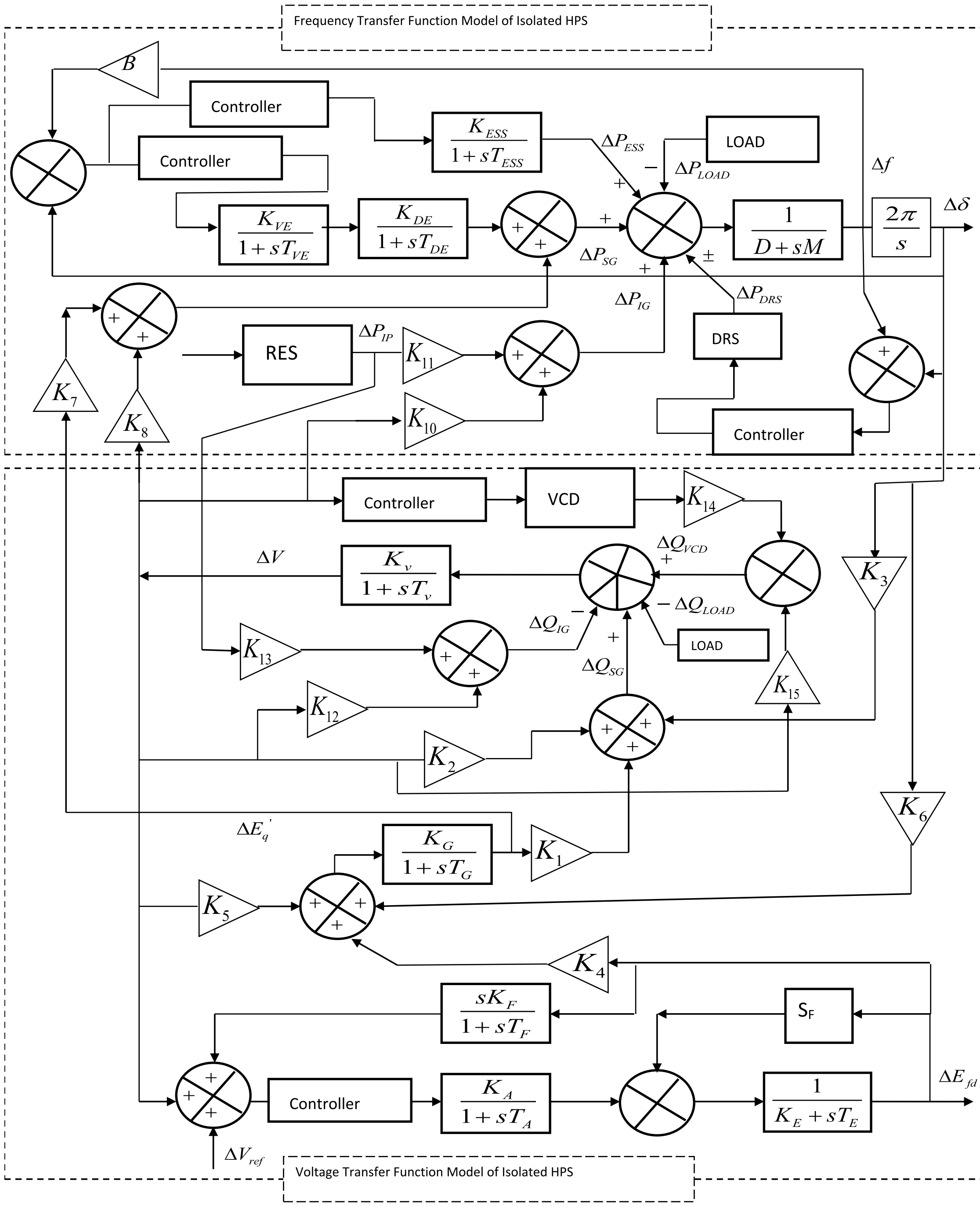

Fig. 3(b). Linear Laplace transfer function model of one isolated HPS (area).

This technique generates the value of initial shot points by the following Eq. (22)

$$x_0 = lb + rand(ub - lb) \tag{22}$$

where, x_0, lb, ub and $rand$ are initial shot point, upper bound, lower bound and the operator to generate the random value in between 0 and 1 respectively.

Explosion of the bombs producing the no. of shrapnel pieces (n_s) causes another place x_{n+1} to bomb;

$$x^f_{n+1} = x^f_{e(n+1)} + \exp\left(-\sqrt{\frac{m^f_{n+1}}{d^f_{n+1}}}\right) x^f_n,\ n = 0, 1, 2, .. \tag{23}$$

$$x^f_{e(n+1)} = d^f_n \text{ x } rand \text{ x } \cos\theta \tag{24}$$

where, x, d, and m are the location, distance and the direction of the exploded shrapnel pieces respectively. θ is the velocity angle of the shrapnel which can be calculated as $\theta = 360°/n_s$. It is dependent on the no. of shrapnel pieces.

In Eq. (22), the second part has been considered to improve the location of the mining point under the influence of the previous best solution. d^f_{n+1} and m^f_{n+1} are distance and direction of the shrapnel pieces respectively can be expressed by the following Eqs. (25) and (26).

$$d^f_{n+1} = \sqrt{(x^f_{n+1} - x^f_n)^2 + (F^f_{n+1} - F^f_n)^2} \tag{25}$$

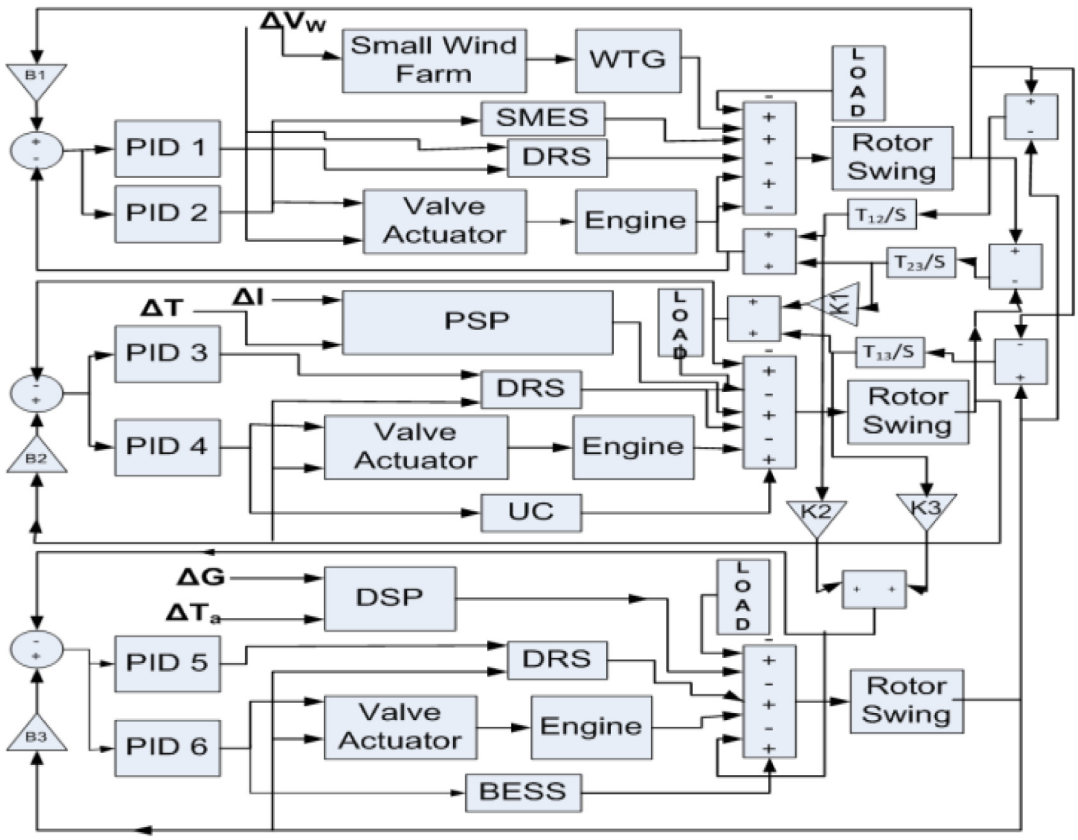

Fig. 3(c). Block diagram of 3-area interconnected hybrid power system.

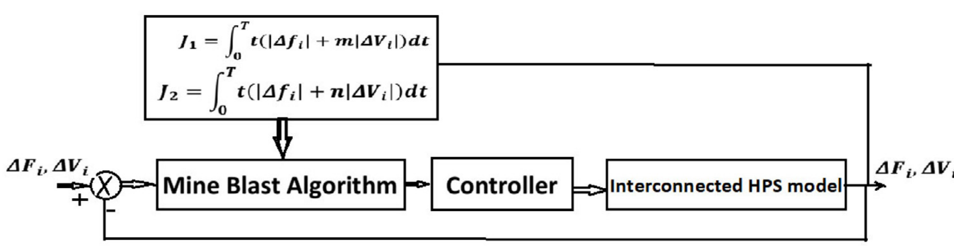

Fig. 3(d). Tuning of controllers' parameters of 3-area interconnected hybrid power system.

$$m_{n+1}^f = \frac{F_{n+1}^f - F_n^f}{x_{n+1}^f - x_n^f}, \quad n = 0, 1, 2, \ldots \tag{26}$$

here, F is defined as the function of x.

Another term, exploration factor defined as μ, is taken into consideration for search space designing, depending on smaller or larger distances. The process of exploration starts when exploration factor is greater than the defined index (k) for iteration number.

The exploration equations can be expressed as:

$$d_{n+1}^f = d_n^f \text{x}(|randn|)^2, \qquad n = 0, 1, 2 \ldots \tag{27}$$

$$x_{e(n+1)}^f = x_{e(n+1)}^f \text{x} \cos\theta, \qquad n = 0, 1, 2 \ldots \tag{28}$$

Here, squaring *randn* provides better search capability for any distances which in turn provides higher exploration ability at very initial stage.

To enhance the search capability globally, the initial separation between the shrapnel pieces is decreased and expressed as:

$$d_n^f = \frac{d_{n-1}^f}{\exp\left(\frac{k}{\alpha}\right)}, \qquad n = 0, 1, 2 \ldots \tag{29}$$

In exploration process, the algorithm considers Eqs. (25) and (26) for the calculation of location and the distances. Exploration factor decides the complexity of the problem. Eq. (29) is considered for the exploitation (i.e., the condition for global optimum solution). Eqs. (25), (26), and (29) imply that the MBA provides the proper balance in between exploration and exploitation to get optimal solution.

4. Simulated results and analysis

A systematic possibility investigation under various scenarios is essential to evaluate the effects of DVR and DRS scheme to reduce the problems related to frequency and voltage of an interconnected system. A frequency–voltage response model has been established and simulated in MATLAB/Simulink software. The analysis has been carried out under all the practical based

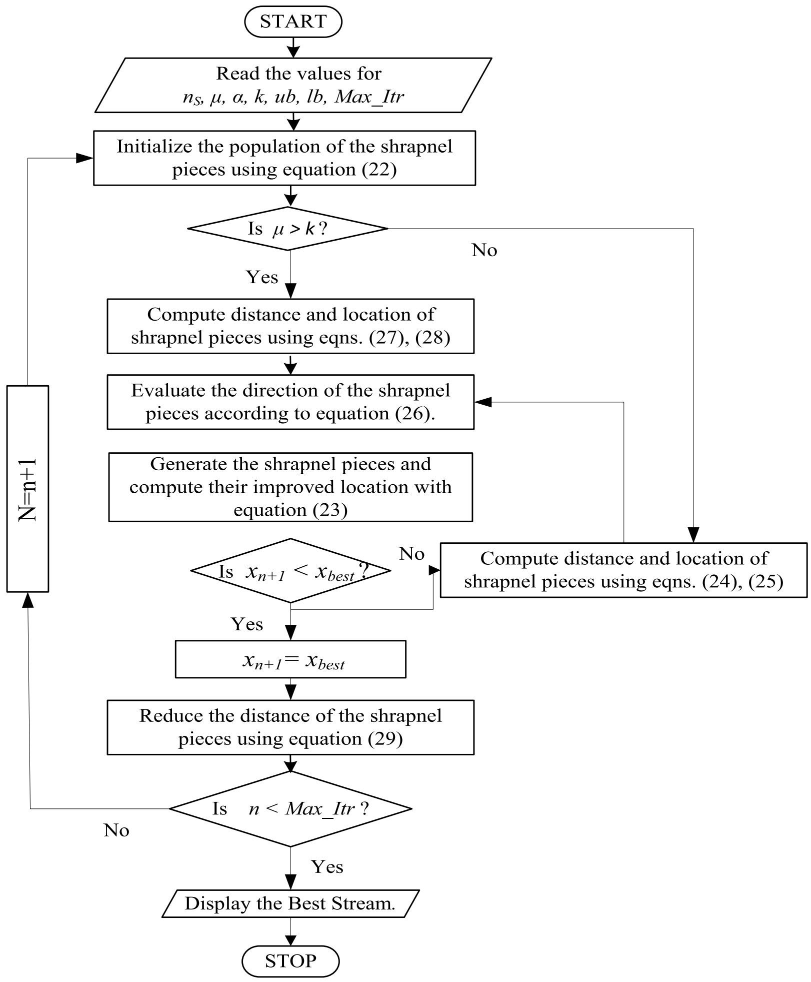

Fig. 4. Flow diagram of Mine Blast Algorithm.

disturbances such as sharp or step load change and the change in intermittent climatic situations. The dynamic responses of the proposed network has been clarifies in this section under the paradigm of the interconnected micro grid. The efficacy and practicality of the proposed network have been investigated under four different scenarios. In the entire scenarios, the controllers' parameters have been tuned through MBA. The efficacy of MBA has been checked over the anticipated system at 5% load perturbation. Flow diagram of MBA for this specific problem has been presented in Fig. 4. In Ranjan et al. (2018) authors have illustrated MBA gives better dynamic responses as compared to GA, PSO and many other techniques. Ref. Sadollah et al. (2013) has also been deliberated MBA in conventional load frequency regulation as one of the essential tools to adjust the Fuzzy based PID controllers (Sadollah et al., 2013). MBA has also been leveraged in Sadollah et al. (2013, 2012) to tune the parameters of the PID controllers to control the frequency fluctuation of the IHPS. This section has proceeded with the selection of proper objective function to minimize the frequency and voltage deviation. Meanwhile, the comparative study among the considered algorithms for optimizing the gains of the controllers has been done.

4.1. Selection for the objective function

There are four diverse objective functions: IAE, ISE, ITSE, and ITAE. These objective functions are considered for optimal selection of the controllers' gains on the basis of minimum frequency deviation. In this section, these objective functions are compared by applying them on the first order P–f transfer function model under DRS. For the selection of the suitable objective function, P–f transfer function model is subjected to 5% change in the load active power at 0 s, and 5 m/s change in wind velocity at 25 s Frequency responses of P–f transfer function model for different objective functions has been shown in Fig. 5(a). The convergence curve for all the objective functions under MBA has been shown in Fig. 5(b). The comparative assessment of the objective functions on the basis of the illustration of the graphs and the their minimum values shown in Table 2 ensures that the ITAE is better as compared to others, therefore all the following case studies are based on the MBA based PID controllers with ITAE as an objective function.

Table 2
Gain values of the controllers for frequency control.

Algorithm		*Gain*	*IAE*	*ISE*	*ISTE*	*ITAE*
MBA(with DRS)	*PID 1*	K_P	*10.628*	*8.665*	*6.698*	*3.552*
		K_I	*4.278*	*5.715*	*7.265*	*5.156*
		K_D	*5.542*	*2.809*	*0.006*	*3.042*
	PID 2	K_P	*7.242*	*2.244*	*3.579*	*0.426*
		K_I	*10.300*	*7.265*	*7.787*	*3.215*
		K_D	*0.025*	*6.565*	*2.609*	*0.049*
	PID 3	K_P	*0.520*	*1.743*	*7.624*	*4.107*
		K_I	*9.924*	*8.665*	*6.009*	*5.657*
		K_D	*2.622*	*1.290*	*0.013*	*2.385*
	$\mathbf{J_{min}}$ (in 10^{-5})		**2.752**	**1.667**	**0.5815**	**0.1658**

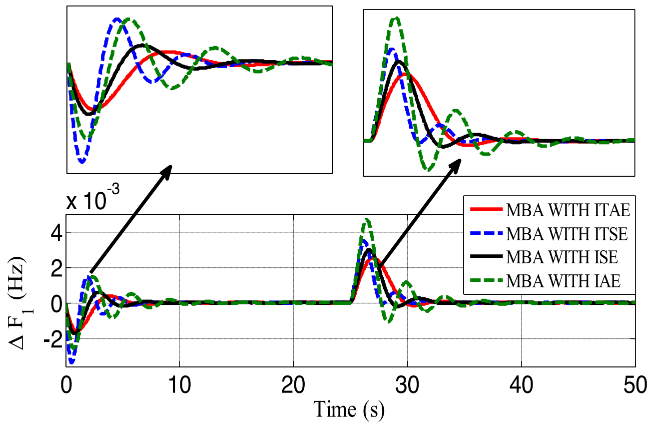

Fig. 5(a). Frequency response of P–f transfer function model under DRS.

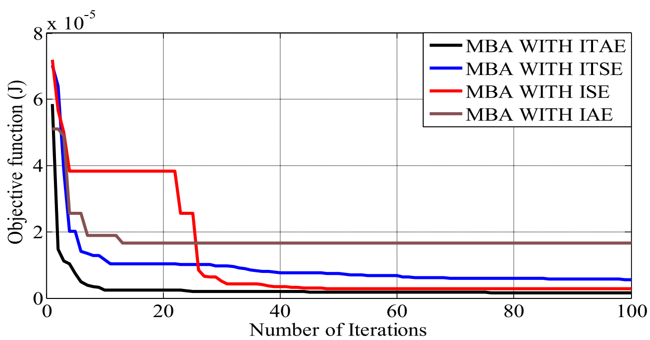

Fig. 5(b). Convergence curve under MBA based PID controllers.

4.2. Direct coupling P–f and Q–V analysis

Case I: ***(a)*** *Separate active power–frequency (P–f) response analysis of the isolated area under DRS*

This case study has considered the area-1 in which WPS is connected as the source of supply and BESS as the energy storage device. The direct relation of active power–frequency has been investigated with and without DRS. Only direct coupling of P–f transfer function model can be developed when K_7, K_8, and K_{12} are set to zero. The P–f transfer function model is subjected to the following disturbances: the wind velocity of the WPS is changed by 5 m/s at 25 s, and the load of 5% is changed at 0 s In P–f transfer function model, only MBA has been considered to optimize the parameters of the PID controllers. The objective function chosen for this case study is ITAE. The active power–frequency response of the isolated hybrid power system is shown in Fig. 6(a). From the illustration, it is evident that the frequency response of the isolated system is better under DRS.

(b) *Separate reactive power–voltage (Q–V) response analysis of the isolated area under VCDs*

The same area-1 is considered for Q–V response analysis. The direct impact of the change in reactive power on the isolated HPS has been investigated under STATCOM and DVR. Direct coupling of Q–V transfer function model can be developed by setting K_3, K_6, and K_9 to zero. The Q–V transfer function model has been subjected to the change in load reactive power with 5% at 0 s PID controller has been tuned with the help of MBA. Their gain values are shown in Table 3. The voltage response of the isolated hybrid power system under STATCOM and DVR illustrated in Fig. 6(b) clearly signifies that the DVR as the voltage compensating unit is better as compared to STATCOM.

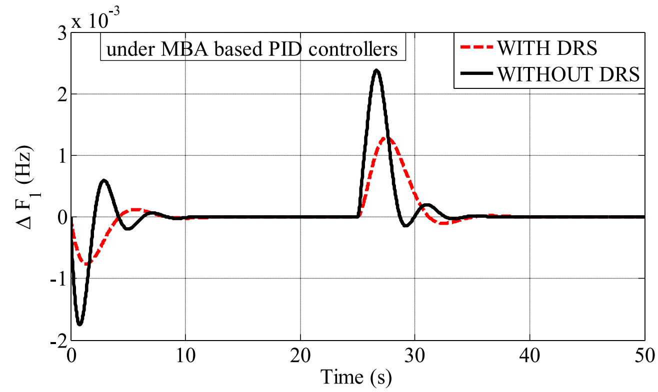

Fig. 6(a). Frequency response for direct coupling analysis.

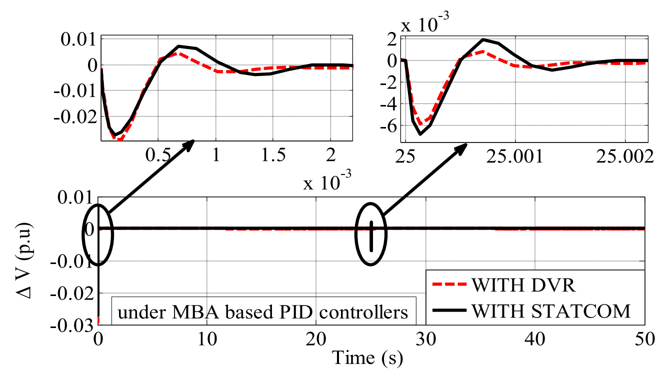

Fig. 6(b). Voltage response for direct coupling analysis.

Table 3
Frequency and voltage deviation and controllers' gains.

Deviation		*STATCOM*	*DVR*	*Gain*		*STATCOM*	*DVR*
F1 (in e−3)	*MUS*	*0.187*	*0.175*		K_P	*1.809*	*1.352*
	ST(s)	*12.24*	*11.75*	*PID 2*	K_I	*2.040*	*3.009*
F2 (in e−3)	*MUS*	*0.295*	*0.280*		K_D	*0.041*	*1.342*
	ST (s)	*13.25*	*12.24*		K_P	*4.001*	*0.015*
F3 (in e−3)	*MUS*	*0.135*	*0.128*	*PID 3*	K_I	*5.017*	*2.092*
	ST	*11.59*	*11.27*		K_D	*3.255*	*2.886*
V1 (in e−3)	*MUS*	*1.245*	*1.106*		K_P	*4.996*	*5.000*
	ST(s)	*5.005*	*4.521*	*PID 4*	K_I	*3.295*	*5.000*
V2 (in e−3)	*MUS*	*1.365*	*1.330*		K_D	*1.620*	*0.016*
	ST (s)	*6.132*	*6.120*		K_P	*1.294*	*2.366*
V3 (in e−3)	*MUS*	*0.997*	*0.752*	*PID 5*	K_I	*4.189*	*1.689*
	ST	*4.529*	*4.362*		K_D	*3.785*	*2.971*
PID 1	K_P	*1.215*	*2.022*		K_P	*1.005*	*4.523*
	K_I	*4.025*	*1.926*	*PID 6*	K_I	*4.996*	*4.125*
	K_D	*2.015*	*0.005*		K_D	*0.744*	*0.002*

4.3. Direct and cross coupling analysis

Case II: *Frequency and voltage responses under STATCOM with 5% change in reactive power in each area and no change in active power.*

The proposed interconnected HPS is developed with the help of first order Laplace transfer function model in MATLAB/SIMULINK environment. The system has been developed in such way so that the simultaneous deviation in frequency and voltage can be analyzed at both reactive and active power change. This case study has considered the IHPS in the presence of STATCOM, where reactive power in each area is changed by 5%. Small perturbation in reactive power occurs at 25 s, 75 s, and

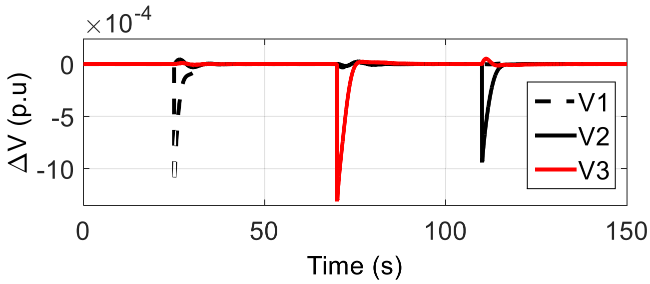

Fig. 7(a). Transient behavior of the system voltage.

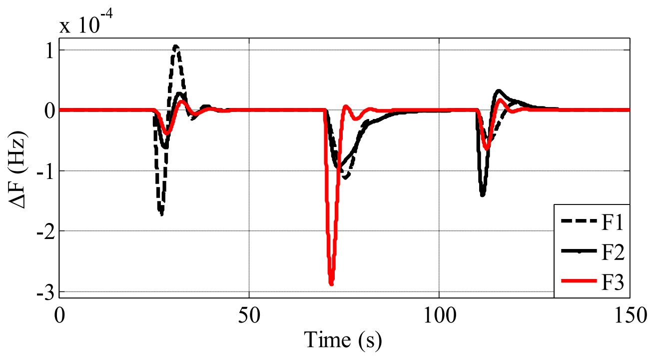

Fig. 7(b). Transient behavior of the system frequency.

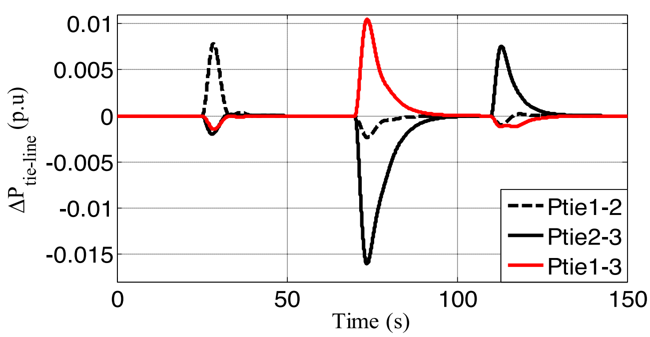

Fig. 7(c). Transient behavior of the tie-line power.

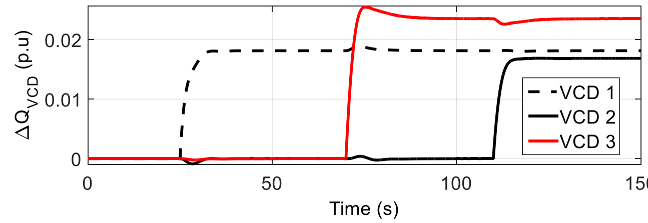

Fig. 7(d). Transient behavior of the voltage compensating devices.

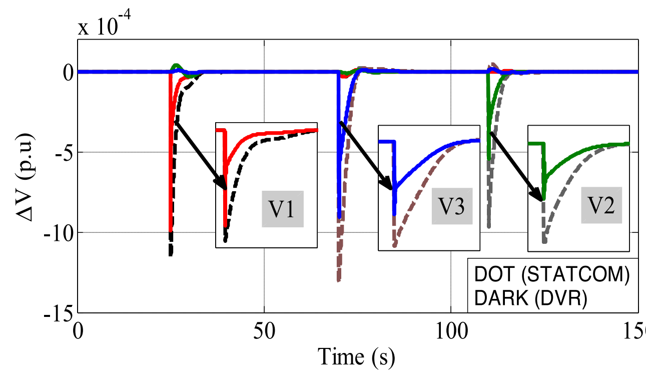

Fig. 8(a). Transient behavior of the system voltage.

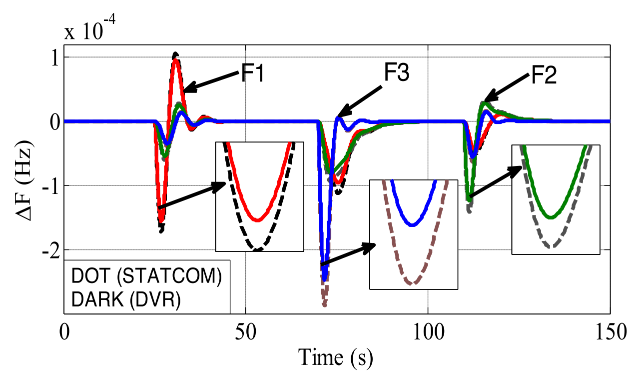

Fig. 8(b). Transient behavior of the system frequency.

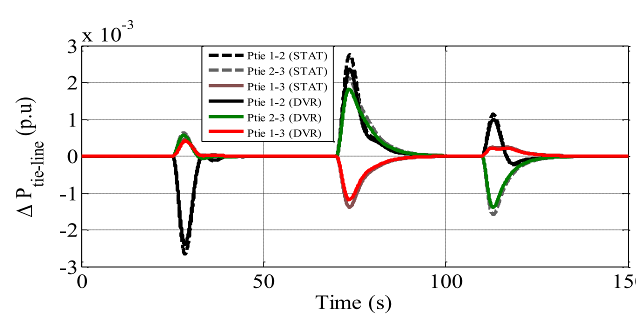

Fig. 8(c). Transient behavior of the tie-line powers.

50 s respectively in area-1, area-2, and area-3. The corresponding voltage deviation to the perturbation has been shown in Fig. 7(a). The voltage deviation has been controlled with the help of VCD like STATCOM. Comparative analysis of the reactive power supplied by the VCDs has been shown in Fig. 7(d). Fig. 7(a) shows the direct relation in between reactive power and voltage as voltage deviation occurs due to the perturbation in the reactive power of the load in each area. But Fig. 7(b) clearly implies that the mismatch in reactive power deviates the frequency as well so it can be interpreted that there is a cross coupling in between reactive power and frequency. Frequency gets deviated from its nominal value at that instant when reactive power changes in each area. Corresponding deviation in the tie line power is shown in Fig. 7(c).

Case III: *Comparative study of frequency and voltage responses under STATCOM and DVR with 5% change in reactive power in each area and no change in active power.*

This case study examines the characteristics of the proposed 3-area interconnected HPS in the presence of VCDs when each area undergoes the change in reactive power at different instant of time. Reactive power change in area-1, area-2 and area-3 has occurred at 25 s 75 s and 50 s respectively. Small perturbation in the load reactive power of only 5% is subjected to each area at above mentioned interval of time to see the effects of voltage deviation in each area. Reactive power change causes voltage deviation which can be clearly figured out from Fig. 8(a). Deviation in voltage shown in Fig. 8(a) signifies the direct coupling in between reactive power and the system voltage. Meanwhile the frequency oscillation in area-1, area-2, and area-3 occurs simultaneously at the same instant of time shown in Fig. 8(b) justifies

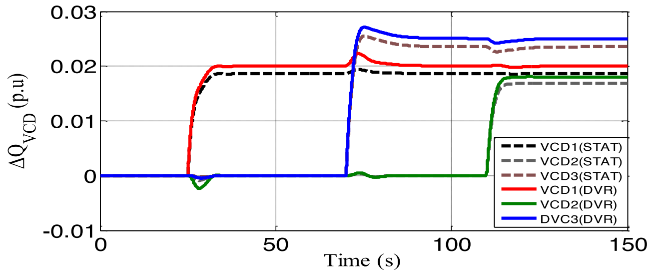

Fig. 8(d). Transient behavior of the voltage compensating devices.

the cross relation in between reactive power and frequency of the small HPS. In Figs. 8(a) and 8(b), shows the order of change in voltage and frequency is somewhat different. The change in voltage has higher order as compared to the change in frequency which explicitly means that there is a loose coupling in between reactive power and frequency whereas strong coupling is there in between reactive power and the system voltage. This case has considered the change in reactive power which causes the voltage deviation that is why the voltage compensating devices (VCDs) are included for proper compensation of reactive power. Here, STATCOM and DVR as compensating devices are used where the effectiveness of the DVR to control the voltage is higher as compared to that of STATCOM which can be clearly seen in Fig. 8(a). Since the isolated HPSs are interconnected with each other that is why there is a tie-line power deviation occurred in the system shown in Fig. 8(c). The reactive power responses of the VCDs are shown in Fig. 8(d). Quantitative analysis of the system responses have been encapsulated in Table 3, and the comparison between STATCOM and DVR is shown in Figs. 8(e) and 8(f) in terms of overshoot and settling time of frequency and voltage.

Case IV: *Comparative study of frequency and voltage responses under DR Scheme*

- *Wind velocity in area 1 is changed by 5 m/s at 25 s.*
- *Solar irradiance in area 2 is changed by 150 W per meter square at 75 s.*
- *Solar irradiance in area 3 is changed by 200 W per meter square at 50 s.*

This case study deals with the simultaneous control of frequency and voltage of the proposed system by controlling active and reactive power mismatch. The proposed system has three area and all the 3 area have different generating units like WPS in area-1, PSP in area-2 and DSP in area-3. In area-1, velocity is changed by 5 m/s which directly affects the active power generation of the WPS. In area-2 and area-3, solar irradiance is changed by 150 W/m^2, and 200 W/m^2 respectively which also lead to the change in active power generation of PSP and DSP. The active power mismatch results in frequency deviation apparently, but in this case also from Fig. 9(a), it can be said that the change in the active power in each area of the interconnected HPS causes frequency deviation and at the same time from Fig. 9(b), it can also be marked that the change in active power deviates the system voltage up to some extent. Above waveform analysis can lead this paper to indicate that there is a loose but cross coupling in between the active power and the system voltage. Frequency and voltage deviations can be seen simultaneously at 25 s, 75 s, and 50 s respectively in area-1, area-2, and area-3. In addition to the simultaneous control of frequency and voltage of the system through proper mathematical modeling active and reactive power in terms of voltage and load angle, the proposed

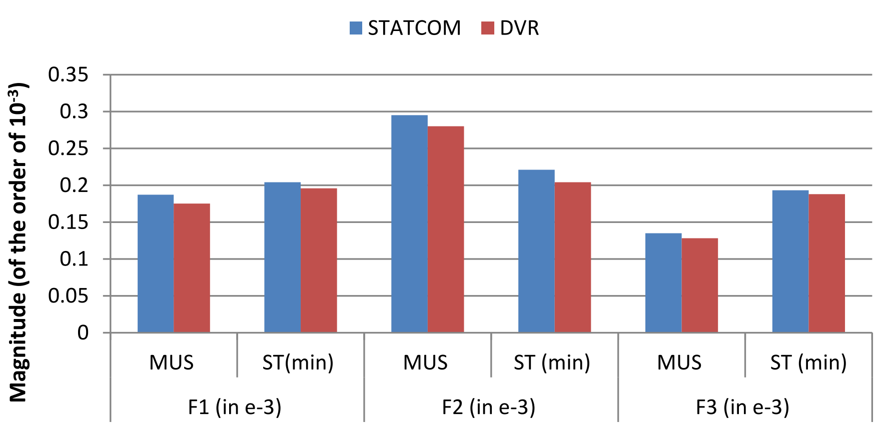

Fig. 8(e). Frequency deviation in terms of MUS and ST.

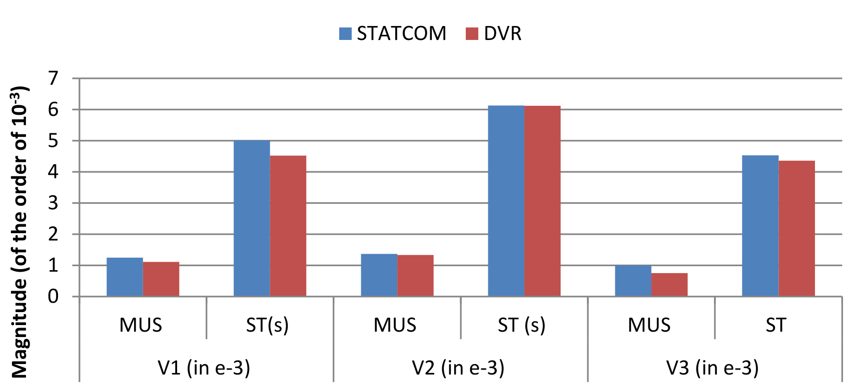

Fig. 8(f). voltage deviation in terms of MUS and ST.

Table 4
Frequency and voltage analysis of the proposed HPS and its controllers' gains.

Deviation		*Without DR*	*With DR*	Controllers gains		*Without DR*	*With DR*
F1 (in e−3)	*MOS*	1.985	1.256	*PID 2*	K_P	0.426	2.135
	ST(s)	14.21	13.02		K_I	3.215	4.448
F2 (in e−3)	*MOS*	2.996	1.560		K_D	0.049	3.245
	ST(s)	12.02	11.00	*PID 3*	K_P	4.107	1.508
F3 (in e−3)	*MOS*	1.220	0.854		K_I	5.000	1.000
	ST(s)	10.20	9.014		K_D	2.385	2.886
V1 (in e−3)	*MOS*	0.385	0.187	*PID 4*	K_P	5.000	4.598
	ST(s)	8.024	7.156		K_I	2.015	5.000
V2 (in e−3)	*MOS*	0.752	0.409		K_D	2.610	0.004
	ST(s)	10.25	9.803	*PID 5*	K_P	3.411	2.457
V3 (in e−3)	*MOS*	0.370	0.185		K_I	4.851	5.000
	ST(s)	7.258	6.244		K_D	0.012	1.791
PID 1	K_P	4.552	3.254	*PID 6*	K_P	1.000	5.000
	K_I	5.000	2.961		K_I	5.000	4.125
	K_D	2.042	4.005		K_D	1.235	0.009

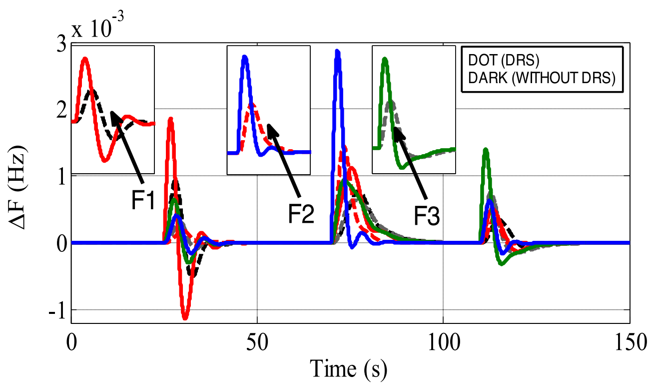

Fig. 9(a). Transient behavior of the system frequency.

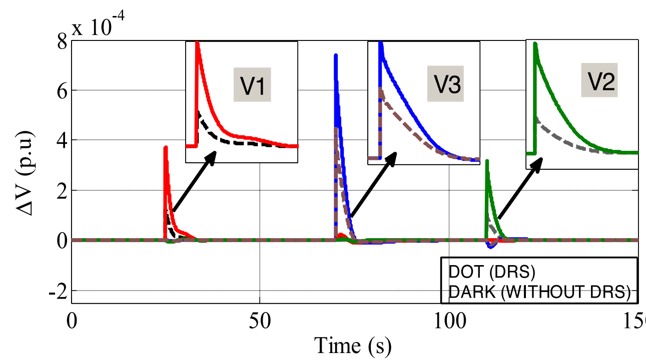

Fig. 9(b). Transient reactive power of system voltage.

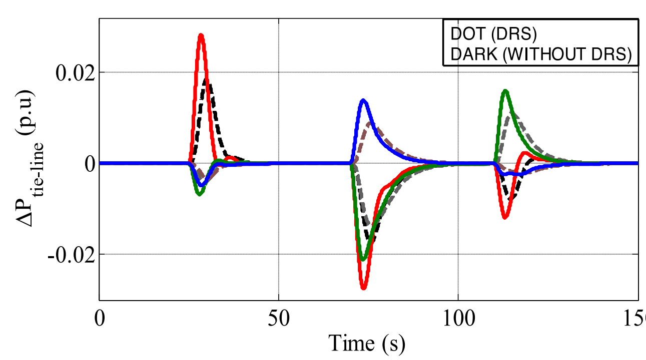

Fig. 9(c). Transient reactive power of tie-line powers.

system has included the demand response (DR) scheme which directly controls the deviation in the frequency shown in Fig. 9(a). The waveform illustration of the frequency with and without DR schemes explicitly signify that the efficacy of DR scheme is significant in suppressing the frequency deviation. This case has considered only DVR as a VCD as DVR has shown the better voltage compensating ability in the earlier two cases. DVR has been connected to the system in the presence and absence of the DR scheme, whose reactive power waveforms have been shown in Fig. 9(b). The tie-line power deviations and reactive power responses of the VCDs are shown in the Fig. 9(c) and Fig. 9(d), respectively. This case study ultimately shows the significance of the DR schemes and the cross coupling relation between the system parameters. Graphical and numerical analysis of the system behavior have been done under DR scheme and encapsulated in the Table 4 and Figs. 9(a)–9(d). The comparative analysis has also been done and shown in Figs. 9(e), and 9(f).

Case V: *Dynamic responses under DR Scheme with uncertainty in wind velocity and solar irradiance.*

The simulated results may be reasonable for a specific system data but not for others. Hence, to check the robustness of the optimized controllers' gains, the uncertain behavior of wind and solar power has been realized through wind velocity variation and the variation in solar irradiances. In area-1, wind velocity is continuously changing which corresponds to almost 5% variation in active power generation whereas solar irradiance is variable in area-2, and area-3 which also corresponds to 5% variation in the power generation. In this case study, the perturbation has been selected up to 5% which can be taken into consideration for small signal analysis. All the areas are subjected to the change in active power continuously which cause frequency deviation of the system shown in Fig. 10(a) and simultaneously system voltage shown in Fig. 10(b) is also deviated from its nominal value which show the cross connection between the parameters like P–V and Q–f. In this case study, DR scheme has been considered to reduce the frequency oscillation as much as possible to maintain the system stability which can be easily observed from Fig. 10(a) and realized the effectiveness of the DR scheme. Finally it can be speculated that the DR increases the frequency stability margin significantly. The change in tie line power due to the disturbance in source power of the generation has been shown in Fig. 10(c). Reactive power responses of the VCDs are also shown in Fig. 10(d) with and without DR scheme which also lead to the conclusion

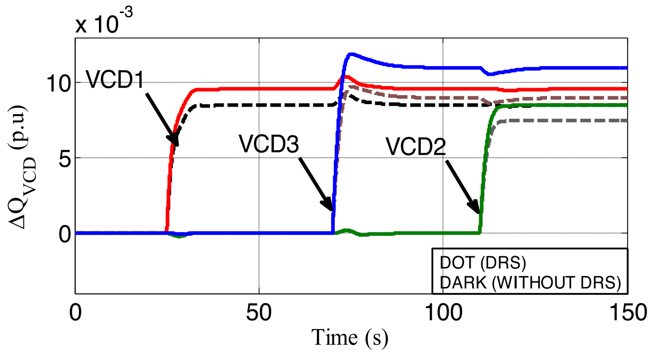

Fig. 9(d). Transient reactive power of VCDs.

that the voltage of the small HPS has the tendency to be affected by the change in active power.

As the system behavior has been analyzed considering above four different cases with the help of MATLAB/SIMULINK to ensure the proposed system adequacy. It can be clearly speculated that the voltage deviation and frequency deviation found in all the cases are within permissible limits in the presence of VCD and DR scheme. The MATLAB waveforms, in fact, figure out the effective use of VCDs and DR scheme in the mitigation of voltage and frequency deviation. At the same time DVR makes the entire system less vulnerable to reactive power changes. Comparison of the system behaviors under different loading and generating condition makes sure that the small HPS has not only the direct relation in between the system parameters like P–f and Q–V but also the indirect relation in between them like P–V and Q–f.

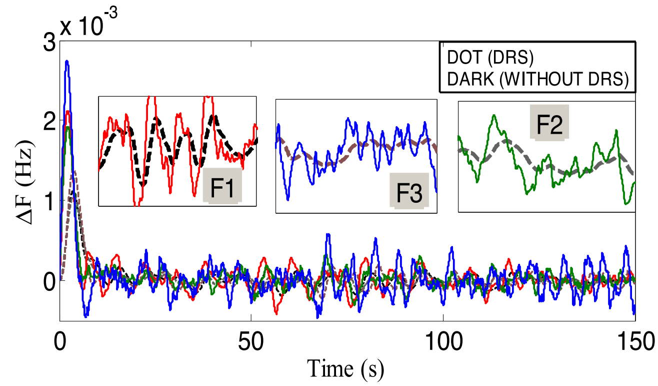

Fig. 10(a). Transient behavior of the system frequency in different areas.

5. Conclusion

This study has highlighted the importance of the indirect relation like P–V, and Q–f along with direct relation like P–f and Q–V for the interconnected hybrid power system (IHPS). The maiden attempt has been made to see the reactive power effect on frequency and active power effect on the system voltage especially in the interconnected hybrid power system (IHPS). For this purpose, Laplace transfer function model of IHPS has been developed mathematically. Four different conditions of the load and the generation are considered, and their Simulink responses have been illustrated to critically analyze the cross-coupling behavior of the proposed IHPS. The quantitative analysis of the waveform in above cases clearly elucidates that the change in

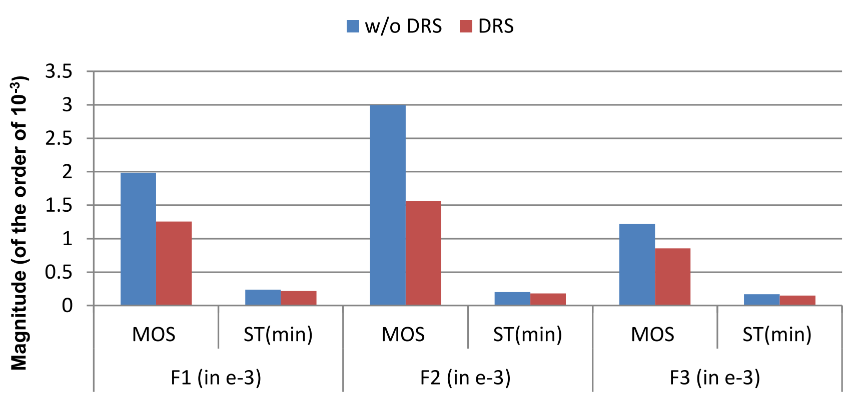

Fig. 9(e). Frequency deviation in terms of MUS and ST.

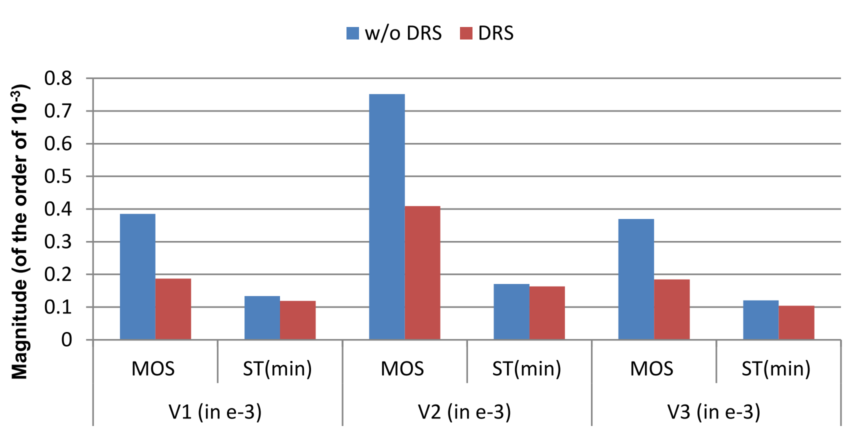

Fig. 9(f). Voltage deviation in terms of MUS and ST.

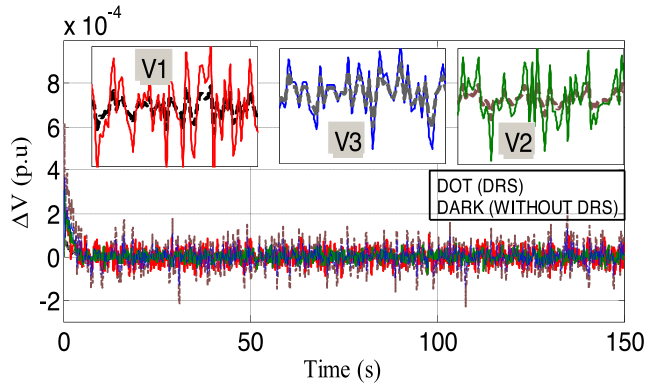

Fig. 10(b). Transient behavior of the system voltage in different areas.

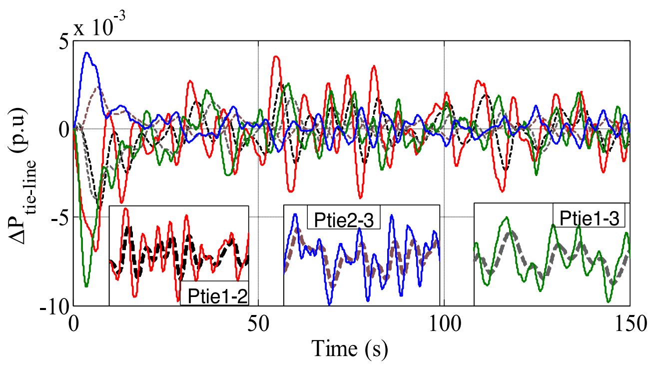

Fig. 10(c). Transient behavior of tie-line powers.

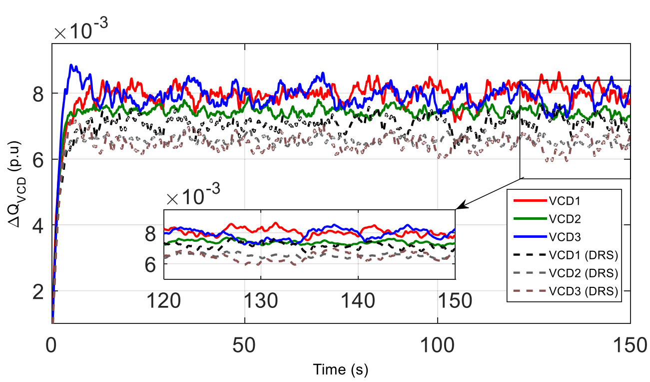

Fig. 10(d). Transient reactive power of VCDs.

reactive power affects the system frequency and change in active power affects the system voltage as well. Moreover, the IHPS has been simulated in the presence of STATCOM and DVR which control the deviation in voltage which can be seen in the above waveforms where DVR performs better as compared to STATCOM. Frequency instability is severe than voltage instability that is why DR scheme has also been introduced to see its effect on the frequency deviation. The quantitative analysis explicitly indicates that the DR scheme is much more effective in controlling the frequency deviation.

CRediT authorship contribution statement

Sudhanshu Ranjan: Conceptualization, Software, Validation, Investigation, Writing – original draft, Writing – review & editing, Visualization, Methodology, Formal analysis, Investigation. **Abdul Latif:** Conceptualization, Software, Validation, Investigation, Writing – review & editing, Visualization, Methodology, Formal analysis, Investigation. **Dulal Chandra Das:** Conceptualization, Writing – review & editing, Resources, Formal analysis, Funding acquisition, Supervision. **Nidul Sinha:** Conceptualization, Writing – review & editing, Formal analysis, Supervision. **S.M. Suhail Hussain:** Conceptualization, Writing – review & editing, Methodology, Formal analysis, Investigation, Supervision. **Taha Selim Ustun:** Conceptualization, Writing – review & editing, Formal analysis, Supervision. **Atif Iqbal:** Conceptualization, Writing – review & editing, Resources, Formal analysis, Supervision, Funding acquisition.

Declaration of competing interest

The authors declare that they have no known competing financial interests or personal relationships that could have appeared to influence the work reported in this paper.

Acknowledgments

"The publication of this article was funded by the Qatar National Library.

This work was made possible by NPRP grant # [13S-0108-20008] from the Qatar National Research Fund (a member of Qatar Foundation). The statements made herein are solely the responsibility of the authors".

References

Avisha, Tah, Das, Debapriya, 2016. Analysis and investigation on direct and cross coupling effect of small isolated and interconnected wind diesel power generating system. IET Renew. Power Gener. 11 (2), 215–227.

Bansal, R.C., Bhatti, T.S., 2008. Small Signal Analysis of Isolated Hybrid Power Systems: Reactive Power and Frequency Control Analysis. Narosa Publishing House, New Delhi, India.

Bao, YQ., Li, Y., Hong, YY., et al., 2015. Design of a hybrid hierarchical demand response control scheme for the frequency control. IET Gener. Transm. Distrib. 9 (15), 2303–2310.

Barik, A.K., Das, D.C., 2019. Proficient load-frequency regulation of demand response supported bio-renewable cogeneration based hybrid microgrids with quasi-oppositional selfish-herd optimization. IET Gener. Transm. Distrib. 13 (13), 2889–2898.

Ellingwood, K., et al., 2019. Anlyzing the benefits of hybridization and storage in a hybrid solar gas turbine plant. Int. J. Sustain. Energy 1–29.

Ellingwood, K., et al., 2020. A novel means to flexibly operate a hybrid concentrated solar power plant and improve operation during non-ideal direct normal irradiation conditions. Energy Convers. Manage. 203, 112275.

Fukami, T., et al., 2004. A technique for the steady-state analysis of a grid-connected permanent-magnet induction generator. IEEE Trans. Energy Convers. 19, 318–324.

Huang, H., Li, F., 2013. Sensitivity analysis of load-damping characteristic in power system frequency regulation. IEEE Trans. Power Syst. 28 (2), 1324–1335.

Hussain, I., et al., 2017. Reactive power performance analysis of dish–stirling solar thermal–diesel hybrid energy system. IET Renew. Power Gener. 11 (6), 750–762.

Ju, Xing, et al., 2017. Recent advances in the PV-CSP hybrid solar power technology. AIP Conf. Proc. 1850.

Latif, A., Das, D.C., Barik, A.K., Ranjan, S., 2020a. Illustration of demand response supported co-ordinated system performance evaluation of YSGA optimized dual stage PIFOD-(1+ PI) controller employed with wind-tidal-biodiesel based independent two-area interconnected microgrid system. IET Renew. Power Gener. 14 (6), 1074–1086. http://dx.doi.org/10.1049/iet-rpg.2019.0940.

Latif, A., Hussain, S.M.S., Das, D.C., Ustun, T.S., 2020b. State-of-the-art of controllers and soft computing techniques for regulated load frequency management of single/multi-area traditional and renewable energy based power systems. Appl. Energy 226 (15), http://dx.doi.org/10.1016/j.apenergy.2020.114858.

Latif, A., Hussain, S.M.S., Das, D.C., Ustun, T.S., Iqbal, A., 2021. A review on fractional order (FO) controllers optimization for load frequency stabilization in power networks. Energy Rep. 7, 4009–4021.

Lee, D.J., Wang, L., 2008. Small-signal stability analysis of an autonomous hybrid renewable energy power generation/energy storage system part I: time domain simulations. IEEE Trans. Energy Convers. 23 (1), 311–320.

Li, Y., Han, M., Yang, Z., Li, G., 2021. Coordinating flexible demand response and renewable uncertainties for scheduling of community integrated energy systems with an electric vehicle charging station: A bi-level approach. IEEE Trans. Sustain. Energy 12 (4), 2321–2331.

Meena, A., Islam, S., Anand, S., Sonawane, Y., Tungare, S., 2017. Design and control of single-phase dynamic voltage restorer. Indian Acad. Sci. 42 (8), 1363–1375.

Othman, Ahmed M., El-Fergany, Attia A., 2018. Design of robust model predictive controllers for frequency and voltage loops of interconnected power systems including wind farm and energy storage system. IET Gener. Transm. Distrib. 12 (19), 4276–4283.

Pourmousavi, SA., Nehrir, MH., 2012. Real-time central demand response for primary frequency regulation in microgrids. IEEE Trans. Smart Grid 3 (4), 1988–1996.

Pourmousavi, SA., Nehrir, M.H., 2014. Introducing dynamic demand response in the LFC model. IEEE Trans. Power Syst. 29 (4), 1562–1572.

Powell Kody, M., et al., 2017. Hybrid concentrated solar thermal power systems: A review. Renew. Sustain. Energy Rev. 80, 215–237.

Praene, Jean-Philippe, et al., 2016. Dish stirling system potential assessment for eight main sites in Madagascar. JP J. Heat Mass Transf. 13 (1), 119–141.

Priyavarthini, S., et al., 2018. An improved control for simultaneous sag/swell mitigation and reactive power support in a grid-connected wind farm with dvr.. Int. J. Electr. Power Energy Syst. 101, 38–49.

Ranjan, S., Das, D.C., Behera, S., Sinha, N., 2018. Parabolic trough solar–thermal–wind–diesel isolated hybrid power system: active power/frequency control analysis. IET Renew. Power Gener. 12 (16), 1893–1903.

Sadollah, A., Bahreinijad, A., Eskandar, H., et al., 2012. Mine blast algorithm for optimization of truss structures with discrete variables. Comput. Struct. 102, 49–63.

Sadollah, A., Bahreinijad, A., Eskandar, H., et al., 2013. Mine blast algorithm: A new population based algorithm for solving constrained engineering optimization problems. Appl. Soft Comput. 5 (13), 2592–2612.

Senjyu, T., Nakaji, T., Uezato, K., et al., 2005. A hybrid power system using alternative energy facilities in isolated island. IEEE Trans. Energy Convers. 20 (2), 406–515.

Shankar, G., Mukherjee, V., 2016. Load frequency control of an autonomous hybrid power system by quasi-oppositional harmony search algorithm. Int. J. Electr. Power Energy Syst. 78, 715–734.

Sharma, P., et al., 2013a. Dynamic stability study of an isolated wind-diesel hybrid power system with wind power generation using IG, PMIG and PMSG: A comparison. Electr. Power Energy Syst. 53, 857–866.

Sharma, P., et al., 2013b. Performance investigation of isolated wind–diesel hybrid power systems with WECS having PMIG. IEEE Trans. Ind. Electron. 60 (4), 1630–1637.

Sitthidet, V., Ngamroo, I., Kaitwanidvilai, S., 2010. Coordinated SVC and AVR for robust voltage control in a hybrid wind-diesel system. Energy Convers. Manage. 51 (12), 2383–2393.

Taqiyeddine, B., et al., 2013. Parabolic trough solar thermal power plant: Potential, and projects development in Algeria. Renew. Sustain. Energy Rev. 21, 288–297.

Wang, S., et al., 2006. Modeling and control of a novel transformer-less dynamic voltage restorer based on H-bridge cascaded multilevel inverter. In: IEEE in 2006 International Conference on Power System Technology. pp. 1–9.

Wang, Jinping, et al., 2019. Thermal performance analysis of a direct-heated recompression supercritical carbon dioxide brayton cycle using solar concentrators. Energies 12, 4358.

Wessels, C., Hoffmann, N., Molinas, M., Fuchs, F.W., 2013. Statcom control at wind farms with fixed-speed induction generators under asymmetrical grid faults. IEEE Trans. Ind. Electron. 60 (7), 2864–2874.

Zhu, Qi, Jiang, Lin, Yao, Wei, Zhang, Chuan-Ke, Luo, Cheng, 2017. Robust load frequency control with dynamic demand response for deregulated power systems considering communication delays. Electr. Power Compon. Syst. 45 (1), 75–87. http://dx.doi.org/10.1080/15325008.2016.1233300.